

Supporting Information

Enhancing CO₂ reduction by suppressing hydrogen evolution with polytetrafluoroethylene protected copper nanoneedles

Pengda An,^{†a,b} Lai Wei,^{†a} Huangjingwei Li,^{†a} Baopeng Yang,^a Kang Liu,^a Junwei Fu,^a Hongmei Li,^a
Hui Liu,^c Junhua Hu,^d Ying-Rui Lu,^e Hao Pan,^f Ting-Shan Chan,^{*c} Ning Zhang,^{*b} and Min Liu^{*a}

^a State Key Laboratory of Powder Metallurgy, School of Physics and Electronics, Central South University, Changsha, 410083. E-mail:
minliu@csu.edu.cn

^b School of Materials Science and Engineering, Central South University, Changsha 410083. Email: nzhang@csu.edu.cn

^c School of Metallurgy and Environment, Central South University, Changsha 410083.

^d School of Materials Science and Engineering, Zhengzhou University, Zhengzhou 450002.

^e National Synchrotron Radiation Research Center, Hsinchu, 30076. Email: chan.ts@nslrc.org.tw

^f Department of Periodontics & Oral Mucosal Section, Xiangya Stomatological Hospital, Central South University, 72 Xiangya Road,
Changsha.

[†] These authors contributed equally to this work.

Experimental Section

1. COMSOL Multiphysics simulations

We used the COMSOL Multiphysics finite-element-based solver to simulate the free electron density on the electrode, the electric field and potassium ion (K^+) density within the vicinity of the electrodes. The 'Electric currents' module was used to solve the free electron density on the electrode under a specific electrode bias potential. Electric field E was computed as the opposite gradient of the electric potential: $E = -\nabla V$.

The electric conductivity of the copper electrode was set to be $5.998 \times 10^7 \text{ Sm}^{-1}$, while the electrolyte conductivity was assumed to be 10 Sm^{-1} . We use Gauss' law for electric field: $\rho = \epsilon_r \epsilon_0 \nabla \cdot E$, where ϵ_0 represents the dielectric function in vacuum, and ϵ_r represents the dielectric function of the materials.

In this simulation, the electrical double layer was modeled using the Gouy–Chapman–Stern model, including a Helmholtz layer and a diffusion layer. A monolayer of surface-adsorbed hydrated cation on the electrode surface in Helmholtz layer speeds up the carbon dioxide reduction reaction (CO_2RR). In the diffusion layer, there are cations and anions diffusing freely in the electrolyte, forming concentration gradients towards and away from the electrode surface.

2. Synthesis of catalyst

Copper (Cu) foil (Alfa Aesar, 99.9%) is ultrasound in acetone, ethanol, water and dilute hydrochloric acid (6 wt%) for 20 minutes in turn, then dry with nitrogen. Cleaned Cu foil was electropolished in 85% H_3PO_4 (Aladdin, GR) under a constant voltage for 600 s at 4 V. then anodized in 3 M KOH (Aladdin, AR) at a constant current condition for 350 s at 4 mA cm^{-2} which formed $\text{Cu}(\text{OH})_2$ nanoneedles.

To coat $\text{Cu}(\text{OH})_2$ nanoneedles with PTFE, which had been soaked in 0.5 wt% PTFE dispersion for 10 minutes. Next transfer to a tube furnace, keeping at $300 \text{ }^\circ\text{C}$ under Ar/H_2 (5%) atmosphere with a heating rate of $5 \text{ }^\circ\text{C min}^{-1}$. The obtain sample abbreviated as CuNNs. Sample without PTFE coating was prepared in the same way, just didn't soaked in PTFE dispersion.

3. Catalyst characterization

Scanning electron microscope (SEM) images were obtained from a FEI Helios Nanolab 600 field emission electron microscope. High-resolution morphology images and microstructure were recorded with a 200 kV FEI Tecnai G2 F20 field emission transmission electron microscope. Fourier transform

infrared (FT-IR) spectra were recorded on Nicolet iS50 spectrometer. Phase of catalyst were characterized using X-ray diffraction (Rigaku Miniflex 600, Cu-K α radiation with $\lambda=1.51484 \text{ \AA}$) with a 2θ range from 5° to 85° and a scan rate of 8° min^{-1} . X-ray photoelectron spectroscopy (XPS) was performed with a Thermo Fisher Scientific K-Alpha⁺ instrument. The X-ray adsorption near edge structure (XANES) were conducted at Taiwan Beam Lines BL01C1, BL07A1, and BL17C1 at the National Synchrotron Radiation Research Center (Hsinchu, Taiwan). The electron-storage ring was operated at 1.5 GeV with a current of 300 mA. A Si (111) double-crystal monochromator was employed for the energy selection with resolution dE/E better than 2×10^{-4} at Cu K-edges. The drop contact angles were measured by the optical contact angle measurement (XG-CAMA) in ambient air at room temperature. The volume of the liquid drop was about $5 \mu\text{L}$. The concentration of K^+ were measured by Dionex ICS-600 Ion Chromatography.

4. Electrochemistry CO₂ Reduction

All the electrochemical test was performed in a sealed H-cell with a typical three-electrode configuration, Ag/AgCl (3.5 M KCl) as reference electrode and $2 \times 2 \text{ cm}^2$ Pt foil as counter electrode, data recorded by Autolab PGSTAT101. Electrocatalysis CO₂RR was performed in 0.1 M KHCO₃ (Aladdin, 99.99%) with 500 rpm stirring, each side of H-cell contain 60 mL electrolyte and 40 mL head space remained. Flow rate of CO₂ (99.999%) maintain 20 sccm during the purge of electrolyte and electrocatalysis. pH of CO₂ saturated 0.1 M KHCO₃ is 6.8, and all potential mentioned is transfer to RHE scale using:

$$E_{RHE} = E_{Ag/AgCl} + 0.2117 + 0.0591 \times pH$$

5. Calculation of faradaic efficiency for product

Gas products were analysis by Gas chromatography (Shimadzu, 2014C) and quantification via external standard method. Each peak in GC corresponds to a product and concentration (V) is proportional to peak area.

$$FE = \frac{V \times Q \times P \times nF}{R \times T \times i_{total}} \times 100$$

Where V is volume concentration from GC, i_{total} is current record by workstation, P is pressure, F is Faradaic constant, 96485 C mol^{-1} , n is the electron transfer number of specific product, R is ideal gas constant, $8.314 \text{ m}^3 \text{ Pa (K mol)}^{-1}$, Q is flow rate, 20 mL min^{-1} , T is temperature.

Liquid products were analysis by Nuclear Magnetic Resonance (NMR). 0.55mL of electrolyte after test

is mixed with 0.05mL Deuterium oxide then test by the NMR. The calculation of FE is as follow:

$$FE = \frac{C_{liquid} \times V \times nF}{Q_{total}} \times 100$$

Concentration (C_{liquid}) was obtain from NMR, V was electrolyte volume, n is the electron transfer number of specific product, F is Faradaic constant, Q_{total} was electric quantity record by workstation. The corresponding quantification curves for gas, liquid products are display in Fig. S1.

6. Measurement of K^+ concentration

The studied electrode was kept under -1.49 V vs. RHE for 90 s, then dipped into 20 mL ultrapure water for 20 times, repeated this process for 10 times. The K^+ concentration in this solution was test by Ion Chromatography (IC).

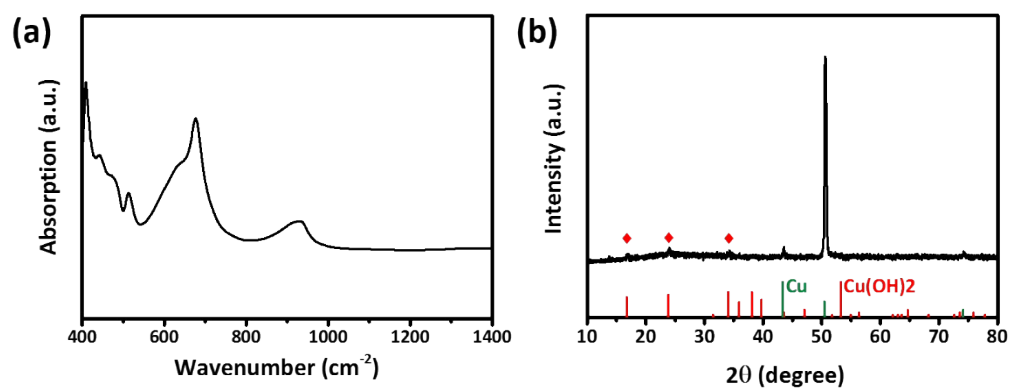


Fig. S1 FT-IR spectrum (a) and XRD pattern (b) of as-obtained CuNNs.

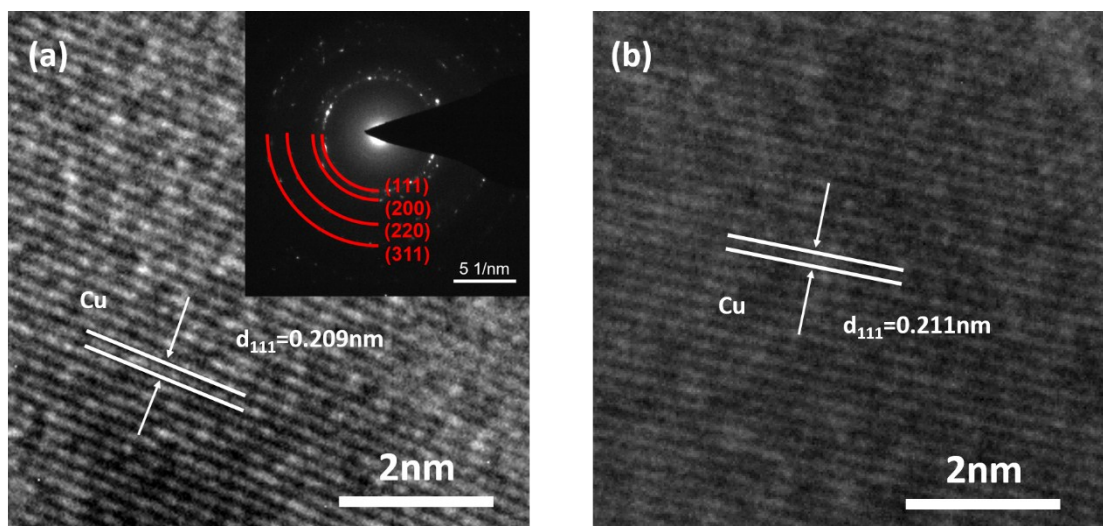


Fig. S2 HRTEM of CuNNs (a) and SAED (insert in Figure S2a) after 1h CO₂RR test under -1.49 V vs. RHE, HRTEM of CuNWs (b) after 1h CO₂RR test under -1.49 V vs. RHE.

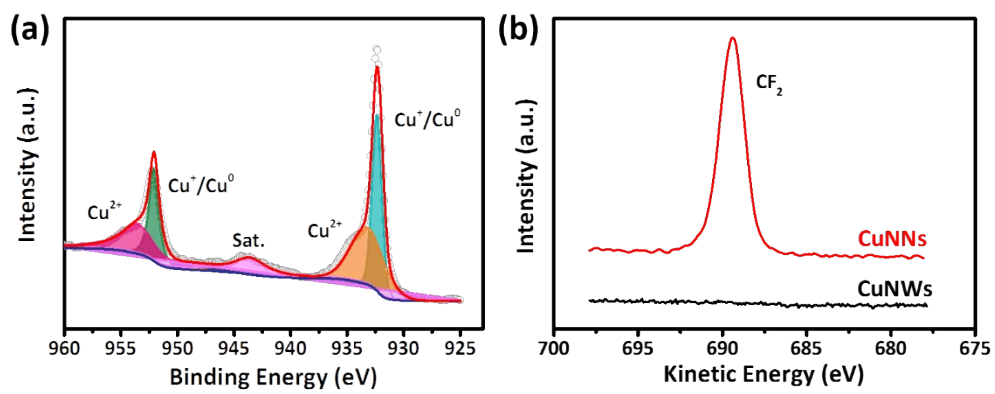


Fig. S3 XPS spectra of Cu 2p region of CuNWs after test (a), F 1s region of CuNNs and CuNWs (b).

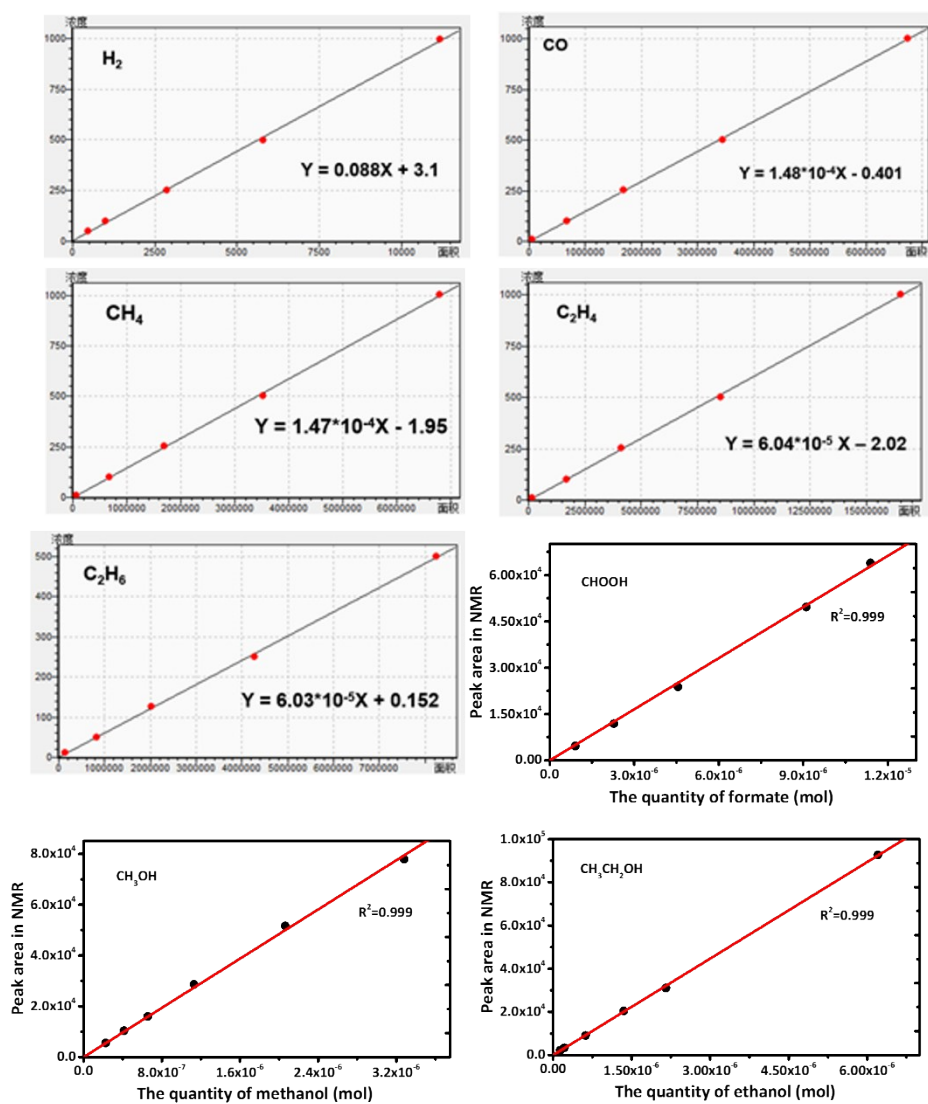


Fig. S4 Quantification curves for gas and liquid products generated during CO₂ reduction.

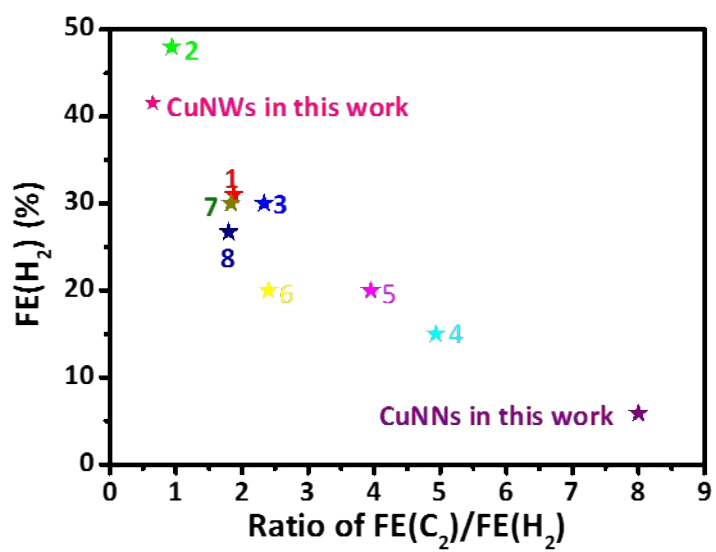


Fig. S5 Comparison of FE(H₂) and ratio of FE(C₂)/FE(H₂) with reported Cu-based catalysts for CO₂RR.

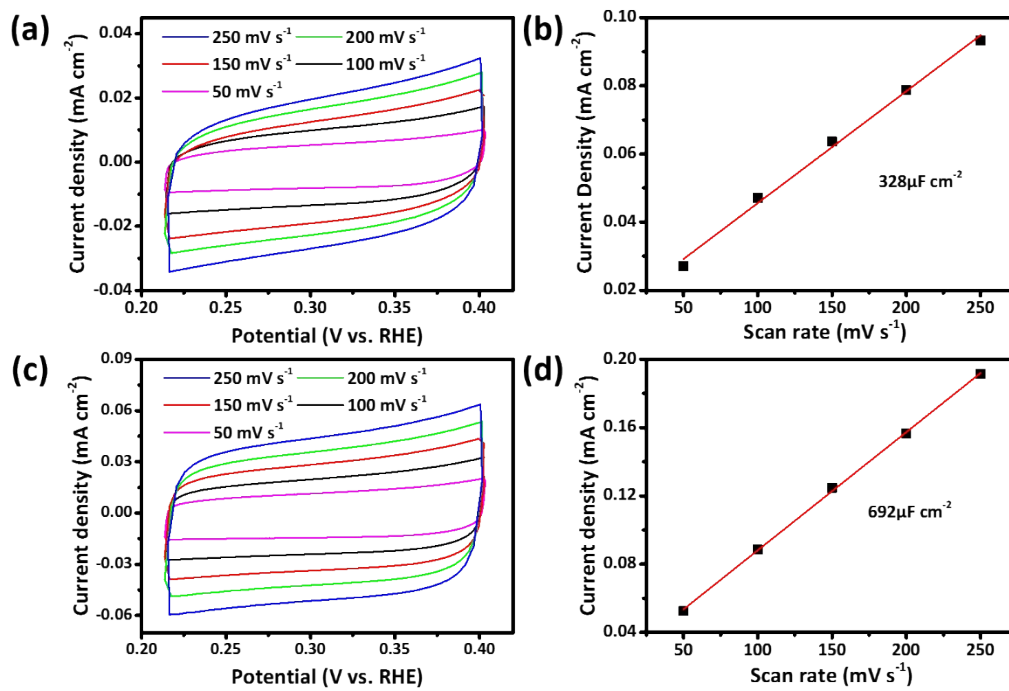


Fig. S6 Cyclic voltammograms of CuNNs (a) and CuNWs (c) at different scan rate (50, 100, 150, 200, 250 mV s⁻¹), measured after electrolysis at -1.49 V vs. RHE for 1 hour. Double-layer capacitance measurement of CuNNs (b) and CuNWs (d).

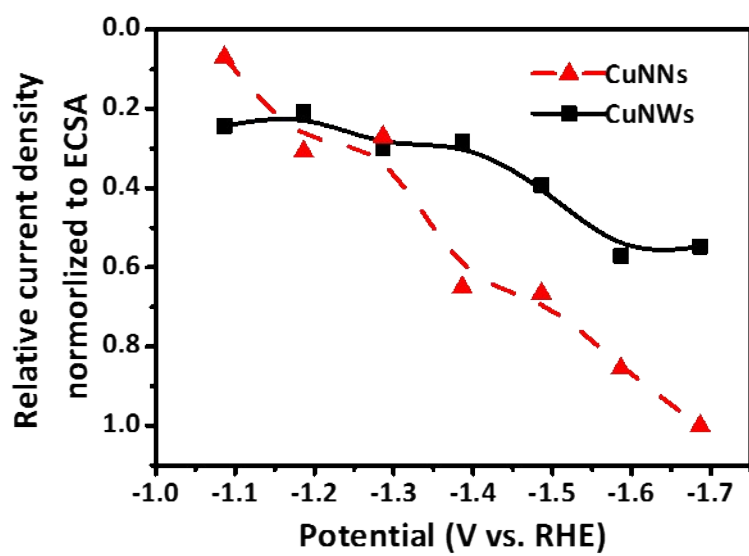


Fig. S7 Current density of CuNNs and CuNWs normalize to ECSA.

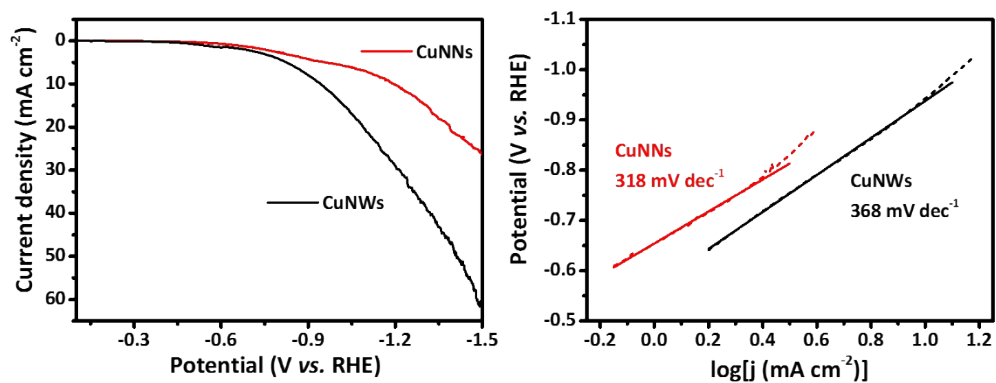


Fig. S8 (a) Linear sweep voltammetry (LSV) curves and corresponding (b) Tafel slope for CuNNs, CuNWs.

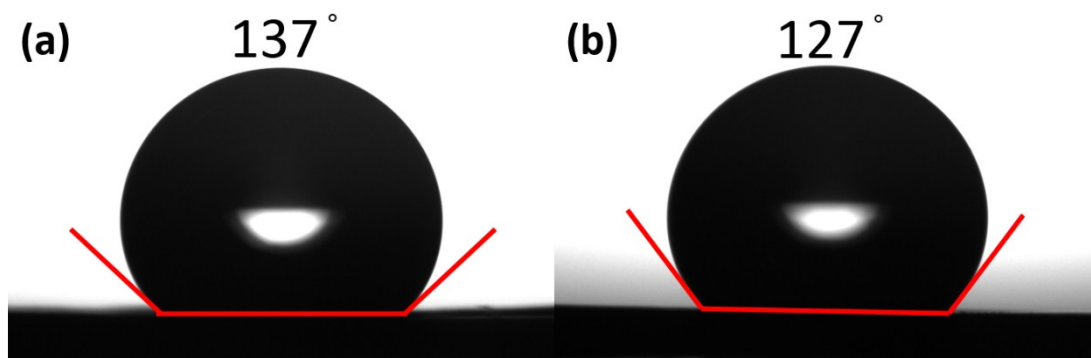


Fig. S9 Contact angel of 0.1 M KHCO₃ aqueous solution on CuNNs (a) and CuNWs (b).

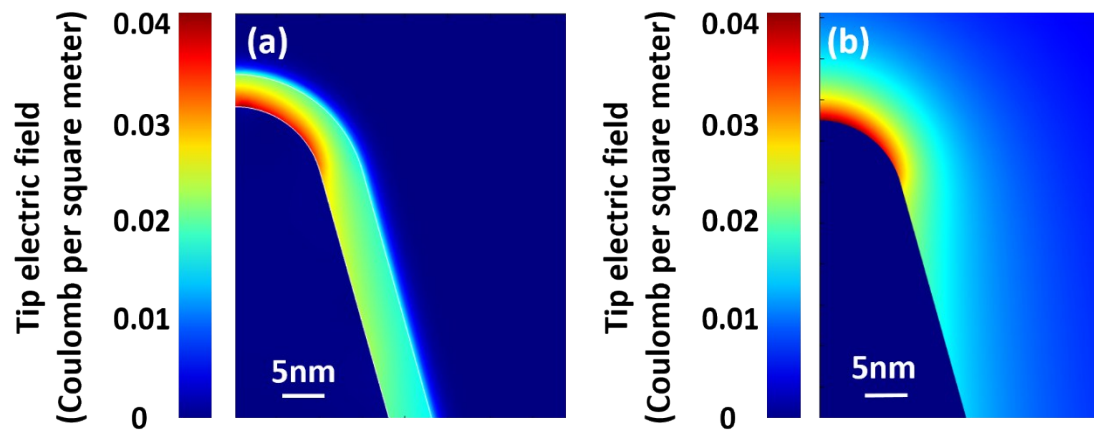


Fig. S10 The comparison between (a) coated and (b) uncoated Cu nanoneedles.

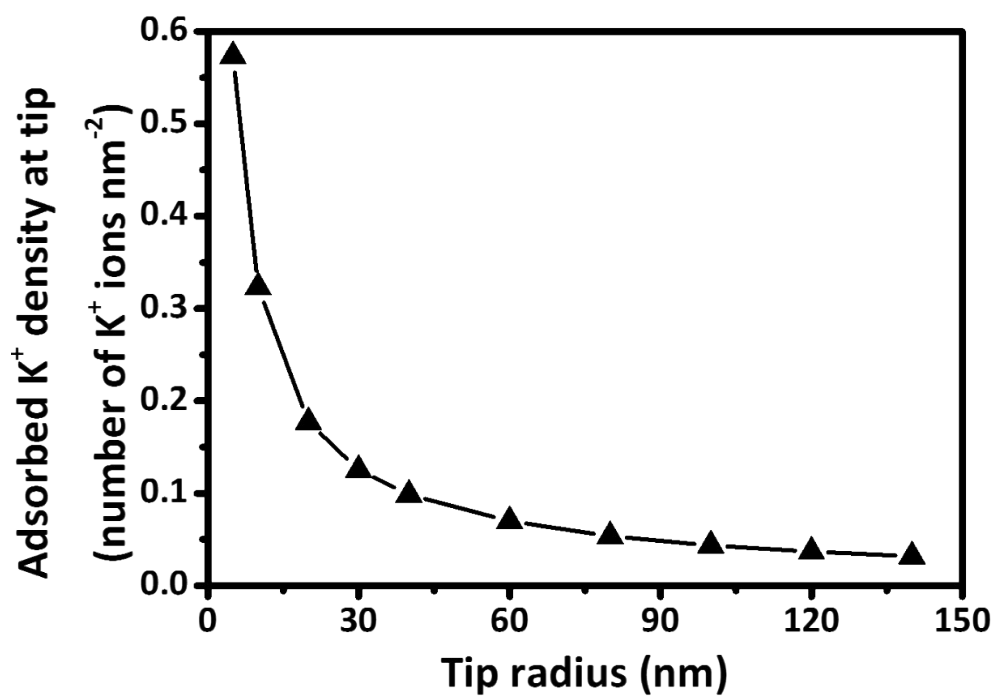


Fig. S11 Simulated adsorbed K⁺ density as functions of radius of the tip.

Table S1 Faradaic efficiency of total products under various potential for CuNNs.

Potential (V vs. RHE)	H ₂ (%)	CO (%)	CH ₄ (%)	COO ⁻ (%)	C ₂ H ₄ (%)	C ₂ H ₅ OH (%)	Total (%)
-1.09	35.79	11.27	0.58	25.87	2.22	23.05	98.78
-1.19	26.82	17.83	4.79	28.26	11.08	12.00	100.78
-1.29	20.32	4.87	12.38	14.03	25.08	13.20	89.88
-1.39	22.00	11.37	7.90	17.67	22.36	14.70	96.00
-1.49	5.87	5.62	32.00	0.77	21.16	25.80	91.22
-1.59	14.69	6.81	15.31	6.76	30.67	21.51	95.75
-1.69	16.43	2.30	11.01	3.60	37.26	17.03	87.63

Table S2 Faradaic efficiency of total products under various potential for CuNWs.

Potential (V vs. RHE)	H ₂ (%)	CO (%)	CH ₄ (%)	COO ⁻ (%)	C ₂ H ₄ (%)	C ₂ H ₅ OH (%)	Total (%)
-1.09	81.60	1.58	0	0	0.27	11.31	94.76
-1.19	37.72	7.44	3.66	26.9	8.17	13.86	97.75
-1.29	42.00	6.71	3.13	19.37	10.34	9.10	90.65
-1.39	29.55	10.21	7.07	24.17	14.60	10.36	95.96
-1.49	41.55	2.24	4.31	11.23	19.27	7.68	86.28
-1.59	28.69	5.45	8.81	11.23	29.68	12.98	96.84
-1.69	24.62	0.94	11.51	4.50	25.87	10.41	77.85

Table S3 Comparison of the FE(H₂) and the Ratio of FE(C₂)/FE(H₂) obtained by CuNNs and CuNWs in this work with those reported Cu-based catalysts in neutral pH aqueous media.¹⁻⁸

No.	Cu catalyst	Potential (V, vs. RHE)	FE of H ₂ (%)	Ratio of FE(C ₂)/FE(H ₂)
This work	CuNNs	-1.49	5.87	8
	CuNWs	-1.49	41.55	0.65
1	Cu nanofibers from CuI	-0.73	31.00	1.87
2	Plasma-modified dendritic Cu	-0.91	48.00	0.94
3	Branched CuO Nanoparticles	-1.05	30.00	2.33
4	Fragmented Cu ₂ O Nanoparticles	-1.1	15.00	4.93
5	B doped Cu nanoparticles	-1.1	20.00	3.95
6	Electrodeposited Copper cube	-0.933	20.00	2.40
7	Electrodeposited Copper dendrites	-1.2	30.00	1.83
8	Cu cube drive from nanoparticles	-0.81	26.70	1.80

REFERENCE

1. H. Wang, E. Matios, C. Wang, J. Luo, X. Lu, X. Hu and W. Li, *Nano Lett.*, 2019, **19**, 3925-3932.
2. F. Scholten, I. Sinev, Dr M. Bernal and B. R. Cuenya, *ACS Catal.*, 2019, **9**, 5496-5502.
3. J. Kim, W. Choi, J. W. Park, C. Kim, M. Kim and H. Song, *J. Am. Chem. Soc.*, 2019, **141**, 6986-6994.
4. H. Jung, S. Y. Lee, C. W. Lee, M. K. Cho, D. H. Won, C. Kim, H. S. Oh, B. K. Min and Y. J. Hwang, *J. Am. Chem. Soc.*, 2019, **141**, 4624-4633.
5. Y. Zhou, F. Che, M. Liu, C. Zou, Z. Liang, P. De Luna, H. Yuan, J. Li, Z. Wang, H. Xie, H. Li, P. Chen, E. Bladt, R. Quintero-Bermudez, T. K. Sham, S. Bals, J. Hofkens, D. Sinton, G. Chen and E. H. Sargent, *Nat. Chem.*, 2018, **10**, 974-980.
6. K. Jiang, R. B. Sandberg, A. J. Akey, X. Liu, D. C. Bell, J. K. Nørskov, K. Chan and H. Wang, *Nat. Catal.*, 2018, **1**, 111-119.
7. P. D. Luna, R. Quintero-Bermudez, C. Dinh, M. B. Ross, O. S. Bushuyev, P. Todorović, T. Regier, S. O. Kelley, P. Yang and E. H. Sargent, *Nat. Catal.*, 2018, **1**, 103-110.
8. D. Kim, C. S. Kley, Y. Li and P. Yang, *Proc. Natl. Acad. Sci.*, 2017, **114**, 10560-10565.